ACS APPLIED MATERIALS & INTERFACES

Research Article

www.acsami.org

Photoelectrochemical Characterization of Hydrogenated TiO_2 Nanotubes as Photoanodes for Sensing Applications

Sheng Li,[†] Jingxia Qiu,[†] Min Ling,[†] Feng Peng,[‡] Barry Wood,[§] and Shanqing Zhang*[,†]

[†]Centre for Clean Environment and Energy, Environmental Futures Centre, Griffith School of Environment, Gold Coast Campus, Griffith University, Queensland 4222, Australia

[‡]School of Chemistry and Chemical Engineering, South China University of Technology, Guangzhou, Guangdong 510640, China

[§]Centre for Microscopy and Microanalysis, The University of Queensland, St. Lucia, Queensland 4072, Australia

Supporting Information

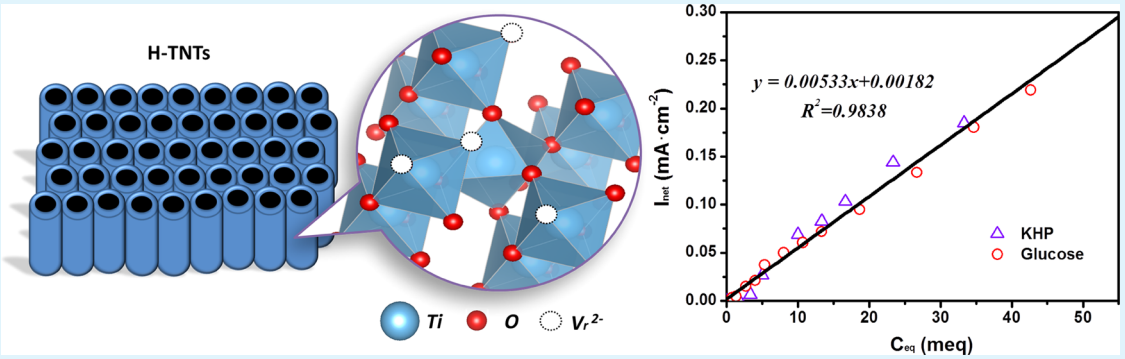

ABSTRACT: In this work, hydrogenated TiO_2 nanotubes (H-TNTs) electrodes were successfully fabricated via the anodization of a titanium sheet followed by a hydrogenation process. Oxygen vacancies were induced in the crystalline structure of TiO_2 nanotubes (TNTs) as shallow donors that enhance the electronic conductivity of the TNTs. This improvement in the electronic conductivity and photoelectrocatalytic (PEC) performance was confirmed and evaluated by a photoelectrochemical characterization. Most importantly, the H-TNTs electrode was able to degrade potassium hydrogen phthalate (strong adsorbent) and glucose (weak adsorbent) indiscriminately. The corresponding photocurrents at the H-TNTs were 2-fold greater than that of the TNTs samples for the same concentrations of the organic compounds. This suggests that the H-TNTs electrode can be a promising sensor for the PEC determination of individual organic compounds or as an aggregative parameter of organic compounds (e.g., chemical oxygen demand).

KEYWORDS: *hydrogenation, TiO_2, nanotubes, sensor, photoelectrocatalysis, oxygen vacancies*

1. INTRODUCTION

Because titanium dioxide (TiO_2) nanomaterials have excellent photoelectrocatalytic (PEC) properties and the potential for use in a wide variety of applications, they have attracted tremendous attention from researchers and have been a dominant PEC material in recent decades.[1,2] To improve their PEC performance, different kinds of TiO_2 materials with larger surface area, more uniform morphology, higher mechanical strength, higher electronic conductivity, and better quantum confinement effects have been synthesized.[3,4] Among various morphologies, 1D nanostructures deliver particularly excellent electronic properties and surface area. TiO_2 nanotubes (TNTs) electrodes possess numerous advantages, such as a large surface area, high light-absorption property, efficient separation of photogenerated holes and electrons, and so forth.[3,5−9] Therefore, they are quite suitable for organic sensing applications.[10]

Although the resistance of TNTs is relatively low compared with that of the TiO_2 nanoparticle films because electron transport is more favorable at the TNTs films,[5,11−13] the electrical conductivity has much room for improvement. Up until now, several methods have been proposed to enhance the conductivity of TNTs, such as doping,[14] filling,[15] decoration,[5] and others. Among these, hydrogenation, a promising modification method, is a simple way to increase donor densities for the improvement of the photocatalytic activity of TiO_2.[7,16−20] In a typical hydrogenation process, the sample is treated at high temperature in an H_2 atmosphere, which allows H_2 to penetrate into the TiO_2 crystal lattice and react with part of the oxygen, see eqs 1 and 2[21]

$$TiO_2 + xH_2(g) \rightarrow TiO_{(2-x)} + xH_2O(g) \quad (1)$$

$$O^{2-}(s) + H_2(g) \rightarrow H_2O(g) + V_r^{2-} \quad (2)$$

Received: August 12, 2013
Accepted: October 1, 2013
Published: October 1, 2013

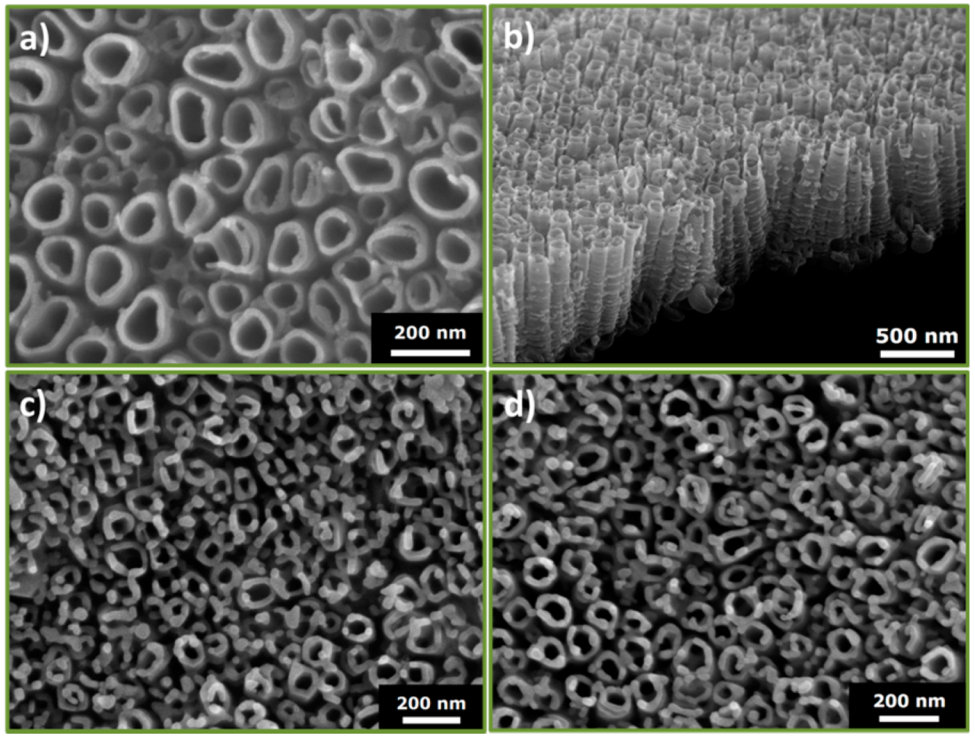

Figure 1. SEM images: (a) top view of pristine TNTs, (b) cross-section view of pristine TNTs, (c) top view of TNTs, and (d) top view of H-TNTs.

where V_r^{2-} refers to a reactive-oxygen vacancy. From a chemical composition point view, this reaction changes the stoichiometric ratio of Ti:O from 1:2 (TiO_2) to 1:2−x ($TiO_{(2-x)}$), leading to so-called oxygen deficiencies. From a crystalline structure point view, this process induces surface disorder. It is believed that the oxygen vacancies are responsible for the generation of midgap energy levels between the valence band and the conduction band. As a result, light absorption is enhanced and extended from the UV to the visible-light region. Besides the contribution of the midgap energy levels, the oxygen vacancies would be considered as shallow donors (charge carriers) in the TiO_2 lattice, which can also account for the conductivity improvement.[22,23] Meanwhile, it was reported that oxygen-deficient TiO_2 with a high carrier concentration would lead to surface plasmon resonance effects and a subsequently improved photocatalytic efficiency.[24,25]

For organic sensing applications, the organics in an aqueous phase could be quantified electrochemically by PEC methods by measuring the photocurrents originated from the degradation process.[26,27] Different oxidation photocurrents at the TiO_2 anode can be associated with the concentrations of the organics. Moreover, different organic compounds ($C_yH_mO_jN_kX_q$) provide various electron-transfer numbers (n) during the exhaustive oxidization according to eq 3

$$C_yH_mO_jN_kX_q + (2y - j)H_2O \rightarrow yCO_2 + qX^- + kNH_3 + (4y - 2j + m - 3k)H^+ + (4y - 2j + m - 3k - q)e^- \quad (3)$$

where X represents a halogen atom and the coefficients y, m, j, k, and q stand for the stoichiometric ratio of elements in the organic compounds. Therefore, n is equal to $4y - 2j + m - 3k - q$ for a specific organic compound.[28−30] This analytical principle has been applied for the determination of chemical oxygen demand (COD) in wastewater[27] as well as for pure organic compound such as glucose and sucrose.[28]

In this work, to improve light absorption, enhance electron conductivity, and boost the PEC degradation performance of the TiO_2 electrodes, a hydrogenated TiO_2 nanotubes (H-TNTs) electrode was prepared by the synthesis of a highly oriented TNTs electrode followed by a subsequent hydrogenation treatment. The PEC reaction resistance of TNTs and H-TNTs thin films were quantitatively characterized using a simple photoelectrochemical method developed in our previous work.[5,31,32] It is expected that the improved conductivity and PEC efficiency of the TiO_2 electrodes will provide higher sensitivity to organic compounds and possibly a larger linear range. Potassium hydrogen phthalate (KHP) and glucose were chosen as representative analytes to demonstrate the analytical performance of the TNTs and H-TNT electrodes.

2. EXPERIMENTAL SECTION

Chemicals and Materials. Titanium (Ti) foil (0.1 mm thick, 99.7% purity) was supplied by Aldrich. Hydrofluoric acid (HF), ethanol, acetone, ammonium fluoride (NH_4F), glucose, KHP, and 1,2,3-propanetriol were purchased from Aldrich without further treatment prior to use. High-purity deionized water (Millipore Corp., 18.2 MΩ cm) was used for preparing the electrolyte solution and for rinsing the samples.

Electrode Preparation. For the fabrication of the pristine TNTs, a 2 × 3 cm^2 Ti foil was cleaned in a sequence of HF (0.5%) for 10 s and deionized water and dried in air. The anodization process was carried out at 25 V for 2 h with a ramp rate of 500 mV/s in a two-electrode compartment, where platinum mesh was used as a cathode and Ti foil as an anode. The electrolyte consisted of 1,2,3-propanetriol, NH_4F (1.0 wt %), and H_2O (15 vol %). Samples were rinsed with deionized water and dried in air at 50 °C. TNTs electrodes were subsequently obtained by annealing the dry pristine TNTs samples in a tubular furnace at 700 °C for 1 h with a heating rate of 5 °C/min in air. The hydrogenation process of the annealed TNTs sample was conducted in a hydrogen atmosphere at 450 °C in a tubular muffle

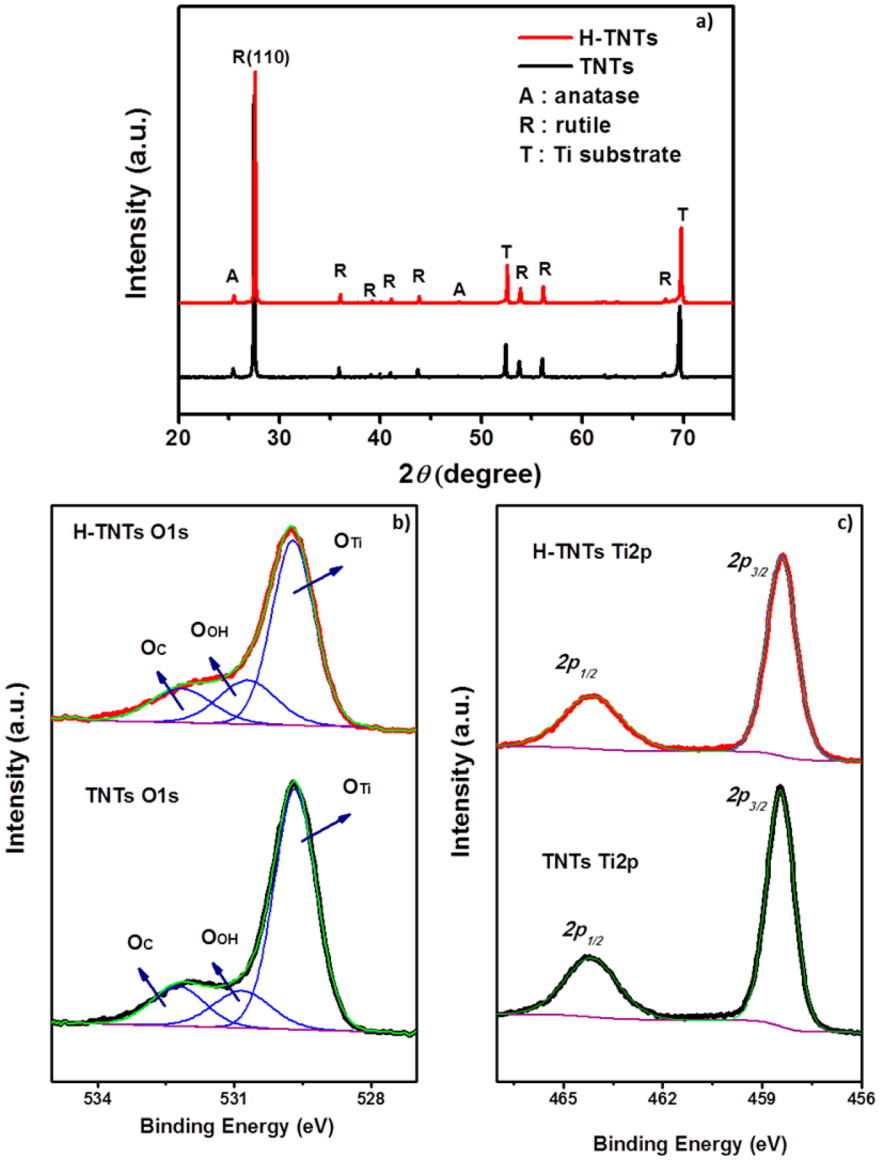

Figure 2. (a) XRD spectrum of TNTs and H-TNTs, (b) O 1s XPS spectra of TNTs and H-TNTs, and (c) Ti 2p XPS spectra of TNTs and H-TNTs.

furnace (MTI Corporation, China) under ambient pressure for 2 h. The resultant electrode is termed the H-TNTs electrode.

Material Characterizations. The morphology of the prepared samples was characterized by scanning electron microscopy (SEM, JSM-7001F). The UV−vis diffusion reflectance (UV−vis/DR) spectra were recorded by a UV−vis spectrometer (U3010, Hitachi). A Kratos Axis ULTRA X-ray photoelectron spectrometer (XPS) incorporating a 165 mm hemispherical electron-energy analyzer was used to analyze the samples. (For details, see the Supporting Information.) The electrochemical characterization was carried out by measuring the photocurrent density of the sample with an electrochemical workstation (CV-27, BAS). In the PEC measurement, a PLS-SXE 300 UV Xe lamp (Changtuo, Beijing) was used as a light source, and a UV band-pass filter (UG 5, Schott) was used to remove the visible and infrared light. A 0.1 M $NaNO_3$ solution was used as the electrolyte, platinum mesh was used as the counter electrode, and a Ag/AgCl electrode was used as the reference electrode. Linear sweep voltammograms (LSVs) were recorded from −0.3 to 2.3 V at a scan rate of 10 mV/s. The PEC determination of organic molecules at the TNTs and H-TNTs electrodes was carried out under a UV illumination intensity of 6.6 mW/cm^2 and a constant applied potential of +0.3 V versus Ag/AgCl. Structural models have been drawn using the Vesta software.[33]

3. RESULTS AND DISCUSSION

Figure 1 shows the surface morphology of the pristine TNTs (Figure 1a), annealed TNTs (Figure 1c), and H-TNTs samples (Figure 1d) as well as the cross-sectional view of pristine TNTs (Figure 1b). In all cases, the TNTs tubes are distributed uniformly and are aligned closely and vertically on the Ti substrates. The average inner diameter of pristine TNTs is ca. 100 nm, whereas the length of all of the TNTs is ca. 900 nm. Upon the annealing processes in air at 700 °C, mild shrinkage in terms of the tubes diameter was observed. The phenomenon is commonly observed because of the growth of the crystal grain during the crystallization process. In comparison, there are no significant morphology changes during the hydrogenation process, suggesting that there are no structural changes between TNTs and H-TNTs.

Figure 2a shows the XRD patterns of the TNTs and H-TNTs electrode. The rutile phase was found to be predominant

as well as a small amount of anatase in both the nanotubes samples. The patterns are similar, and both of the samples clearly exhibit the crystalline peaks of anatase and rutile. At 700 °C, the TNTs are apparently mixed-phased, and after hydrogenation the basic crystal structure is not reformed. It should be noted that the mixed-phase TiO_2 electrode can be applied for PEC sensing applications in a more effective and indiscriminate manner because of the longer lifetime of the photoholes.[34]

XPS survey spectra of the TNTs and H-TNTs (Figure S1) illustrate the presence of O, C, and Ti for both of the samples. High-resolution O 1s and Ti 2p XPS spectra of the TNTs and H-TNTs are displayed in Figure 2, panels b and c, respectively. No obvious peaks shifts were observed after all of the data were referenced by the C−C peak (284.8 eV). The O 1s region in Figure 2b illustrates the presence of three components that are attributed to O−Ti (O_{Ti}), a surface OH group (O_{OH}), and O−C (O_C). The Ti $2p_{3/2}$ and Ti $2p_{1/2}$ peaks in Figure 2c demonstrate the presence of Ti−O in TiO_2, which is in line with the literature.[16,20] The atom percentages (at %) of O and Ti can be quantified by eq 4[35] according to the peak areas at various binding-energy positions of the TNTs and H-TNTs samples and are shown in Table 1.

$$Atom_i\ \% = \frac{Area_i/RSF}{\sum Area_i/RSF} \times 100\% \quad (4)$$

Table 1. Atom percentages of the O 1s and Ti 2p peaks determined by the XPS analysis.

name		TNTs position (eV)	TNTs at %	H-TNTs position (eV)	H-TNTs at %
O 1s	O_{Ti}	529.666	52.54	529.711	45.97
	O_{OH}	530.831	11.26	530.706	14.95
	O_C	532.236	11.29	532.159	12.29
Ti 2p	$2p_{3/2}$	458.453	16.81	458.425	17.53
	$2p_{1/2}$	464.158	8.10	464.127	9.251
O_{OH}:O 1s		15.0%		20.4%	
O_{Ti}:Ti 2p		2.11:1		1.72:1	

where RSF stands for relative sensitivity factor. After hydrogenation, the atom percentage of O_{OH} atoms among all O 1s atoms increased from 15.0 to 20.4%, suggesting that hydrogen reacted with TiO_2 at the TNT surface and produced more hydroxyl groups on the surface. Most importantly, the stoichiometric ratio of O_{Ti}:Ti 2p atoms of the TNT and H-TNT samples were 2.11:1 and 1.72:1, respectively. The significant decrease in the ratio demonstrates the formation of oxygen vacancies during the hydrogenation process. Under normal circumstances, the conductivity of the semiconductor relies on either donating electrons to the conduction band or the valence band receiving holes. In the presence of oxygen vacancies, more dopants lead to the increase of the charge-carrier density, thereby reducing the resistance. Overall, the vacancies produced via the hydrogenation process can provide more charge carriers; consequently, the electrical conductivity could be improved.

The UV−vis/DR spectra of the TNTs and H-TNTs are shown in Figure 3a. They can absorb light with a wavelength from 380 to 420 nm, which partly belongs to visible light. It can also be observed that the H-TNTs sample has a stronger UV absorption than the TNTs sample. The band gaps of the H-TNTs and TNTs can be calculated from the relationship between the absorption coefficient (α) near the absorption edge and the optical band gap (E_g), as shown in eq 5

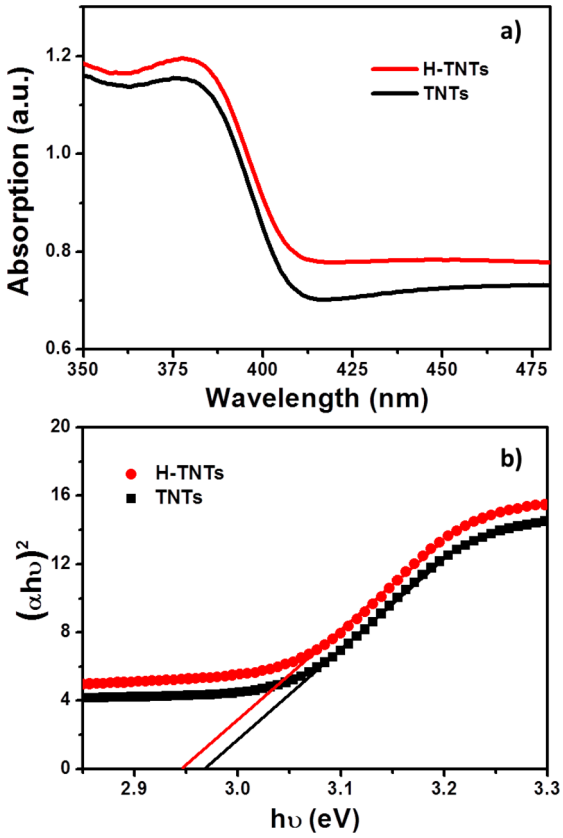

Figure 3. (a) UV−vis/DR spectra of TNTs and H-TNTs and (b) plots of the direct optical band gaps of TNTs and H-TNTs.

$$(\alpha h\nu)^2 = A(h\nu - E_g) \quad (5)$$

where α is absorption coefficient, h is Planck's constant, ν is frequency of vibration of the light, A is the proportional constant, and E_g is the band gap.[36] In Figure 3b, $h\nu$ is plotted versus $(\alpha h\nu)^2$, and the direct optical band gaps of TNTs and H-TNTs could be deduced from the extrapolation of the linear portion of the plots at $\alpha = 0$. The band gap of H-TNTs is 2.95 eV, narrower than that of TNTs (2.97 eV). This confirms that the hydrogenation process could narrow the band gap of the semiconductor, enhance the light-absorption properties, and possibly improve PEC performance.[17]

The PEC characteristics of the TNTs and H-TNTs electrodes were studied by oxidizing water in the PEC cell to confirm the effect of hydrogenation on the PEC activity. Figure 4 shows a series of LSVs obtained from the electrodes in $NaNO_3$ solution under various UV intensities. In the dark, only a negligible current could be observed for both of the electrodes, suggesting that water cannot be electrochemically oxidized by these electrodes in this potential range (−0.3 to +2.3 V). Under UV illumination, the photocurrent increased with the increasing potential before leveling off to a steady photocurrent. The photocurrents of the H-TNTs are almost 2-fold higher than that of the TNTs, confirming that the oxygen vacancy is playing a positive role on the PEC performance.

For the TNTs electrode, the PEC reaction resistance is one of the most important parameters for its application. Different from typical Ohmic resistance, PEC reaction resistance is an

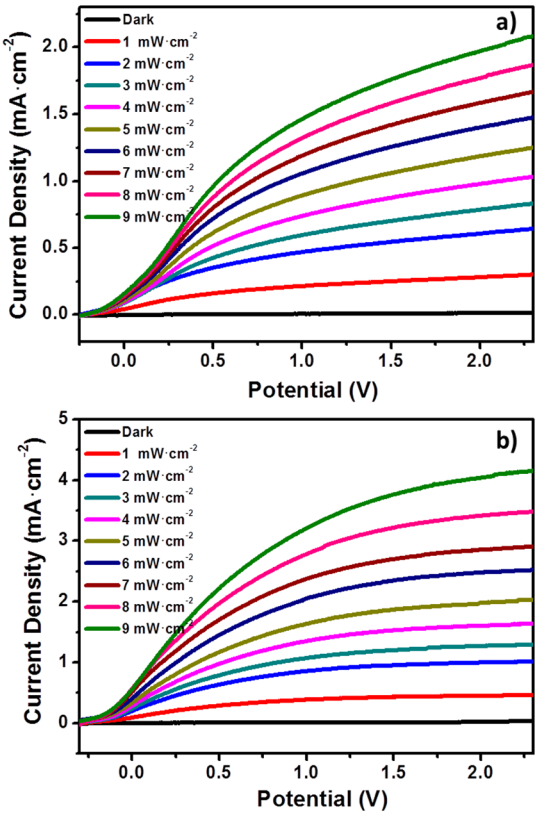

Figure 4. LSVs of (a) TNTs and (b) H-TNTs electrodes in a 0.1 M $NaNO_3$ solution under varied UV-light intensities.

intrinsic property of the electrode during the PEC reaction. A lower PEC reaction resistance of the TiO_2 electrode is apparently beneficial to the separation of photoelectron/hole pairs and a high photoelectric conversion efficiency. To characterize the photoelectron transport property of the TiO_2 thin films, a PEC characterization developed in our previous work[5,31,32] was conducted to evaluate quantitatively the change of the PEC reaction resistance resulting from the hydrogenation process. A series of LSVs were performed under UV illumination at different light intensities (Figure 4a,b). With the increase of the applied potential bias, the photocurrent (I_{ph}) ascends monotonically before leveling off and reaching a saturation photocurrent (I_{sph}) under a given light intensity.

Therefore, the LSV curve can be divided into two parts, the linear increasing part and the saturated part. The former part indicates that photoelectron transport within the TiO_2 photoanodes is the limiting step of the photocurrents. It is similar to the response of a resistor under varying potentials. The saturated part suggests that the interfacial reaction at the TiO_2 surface is the limiting step for the overall process. The potential applied on the TNTs electrode is able to remove all of the electrons generated in the PEC process at the TiO_2 surface in this part.

Here, R is assumed to be the overall resistance of the PEC system, and it consists of two parts: a variable resistance (R_1) and an intrinsic resistance (R_0). Because there is a linear $I-V$ relationship of the PEC curve in which the electron transport inside the photocatalyst layer is a controlling step, Ohm's law is used for calculating the total R here ($R=\Delta E/\Delta I$). The physical meaning of the slope is the sum of R_1 and R_0.

$$R = R_1 + R_0 \quad (6)$$

R_1 is independent of the potential but is relevant to the parameters, such as the types and concentrations of electron scavengers and the light intensity, that may affect the interfacial processes. Therefore, it can be expressed by I_{sph} ($R_1 = k/I_{sph}$) as eq 7:

$$R = k/I_{sph} + R_0 \quad (7)$$

R_0 is an intrinsic property of the semiconductor photo anode that is independent of experimental conditions. It embodies TiO_2 crystal boundary resistances and the resistances at the TiO_2/conducting substrate interface during electron transport. The R value could be calculated by the slope of the linear section, which is selected by a specially designed program (Matlab software). After linear regression fitting, the R values obtained were plotted against $1/I_{sph}$, giving an excellent linear regression equation as eq 7 (Figure 5a,b), and the R_0 values can

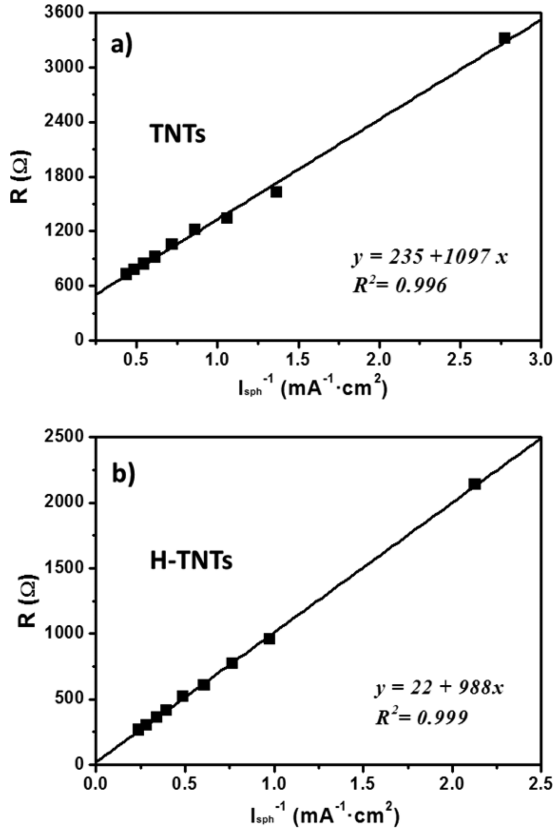

Figure 5. Relationships between the calculated resistance and inverse saturation photocurrent for (a) TNTs and (b) H-TNTs photoanodes. The data were derived from Figure 4, panels a and b, respectively.

be read when the k/I_{sph} value of the fitting plot reaches zero. The R_0 values for the TNTs and H-TNTs photoanodes are 235 and 22 Ω, respectively. The significant difference suggests that after hydrogenation the resistance belonging to the TNTs decreased because of the defects from the oxygen vacancies.

PEC degradation of organic compounds (eq 3) is an effective way to characterize the PEC activity of nanostructured TiO_2 electrodes. In the PEC reaction, the oxidation of organic compounds at the photogenerated photoholes is commonly started from the adsorption of the organic compounds at the TiO_2 surface. The adsorption behavior of the organic compounds might affect the photocatalytic oxidation efficiency significantly.[37] On the basis of the adsorption strength to the

TiO_2 surface, organic compounds can be classified into two categories:[27] weak adsorbents (such as hydroxyl organic compounds; e.g., glucose, phenols, ethanol, etc.) and strong adsorbents (such as organic compounds containing a carboxylic function group; e.g., phathalic acid, glutaric acid, malonic acid, etc.). In this work, glucose and KHP were used as delegates for weak and strong adsorbents, respectively. Because KHP is chemically stable and could even poison the surface of some TiO_2 electrodes,[38,39] it is a tough chore to degrade KHP. The photocurrents were tested under a constant applied potential of +0.30 V in 0.1 M $NaNO_3$. The dark current is approximately zero. Under UV-light illumination, there is a stable background current (I_{blank}) resulting from water oxidation at the surface of the electrode. Different steady-state photocurrents (I_{ss}) can be detected for organic compounds with diverse concentrations, and a net steady-state current (I_{net}) can be obtained by subtracting I_{blank} from I_{ss}.

$$I_{net} = I_{ss} - I_{blank} \quad (8)$$

Because I_{net} represents the oxidation rate of the corresponding organic compounds,[27] it can be used to characterize the PEC activity of the electrode for the oxidation of a certain organic compound. Additionally, I_{net} can be used for the determination of the concentrations of organic compounds under the same experimental conditions. In particular, calibration curves of I_{net} values versus the concentration of glucose or KHP for TNTs and H-TNTs are plotted in Figure 6. As shown in Figure 6a, I_{net} values for glucose and KHP (Figure 6b) at the H-TNTs were more than 2-fold higher than that at the TNTs, suggesting that the H-TNT possesses a higher PEC activity than the TNTs. Also, Figure 6a illustrates that an almost perfect linear relationship of the I_{net} values of the H-TNTs electrode can be clearly observed from 0 to 2.0 mM because the mass transport of the organic compounds was the limiting step. After 2.0 mM, the photocurrents became steady because mass transfer of the organics at the surface of H-TNTs is no longer a limiting step; instead, the oxidation reaction of the organic compounds is a limiting step. In other words, it is reaching the oxidation capacity of the electrode. Meanwhile, although the I_{net} value at the TNTs electrode also went up with the increasing glucose concentration, a well-defined linear range was not observed (Figure S2). In contrast, stronger signals from a clearer linear area have been obtained from the H-TNTs electrode.

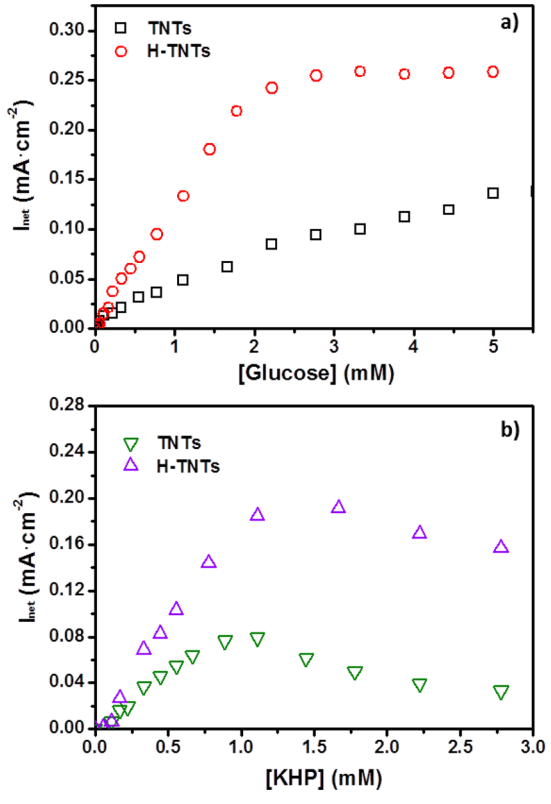

Figure 6. Plot of I_{net} against different concentrations of (a) glucose and (b) KHP for TNTs (black) and H-TNTs (red).

For the oxidation of KHP, the H-TNTs electrode demonstrated not only a 2-fold higher sensitivity than that of the TNTs electrode but also a wider linear range: 0−1.2 and 0−0.9 mM for the H-TNTs and TNTs electrodes, respectively. This implies that hydrogenation bestows the H-TNTs electrode with a better analytical performance in terms of its sensitivity and linear range for both types of organic compounds.

More interestingly, the H-TNTs electrode shows a higher sensitivity to KHP than to glucose when the I_{net} values are plotted against the concentrations of glucose and KHP in the same graph (Figure 7a). This resulted from a larger oxidation

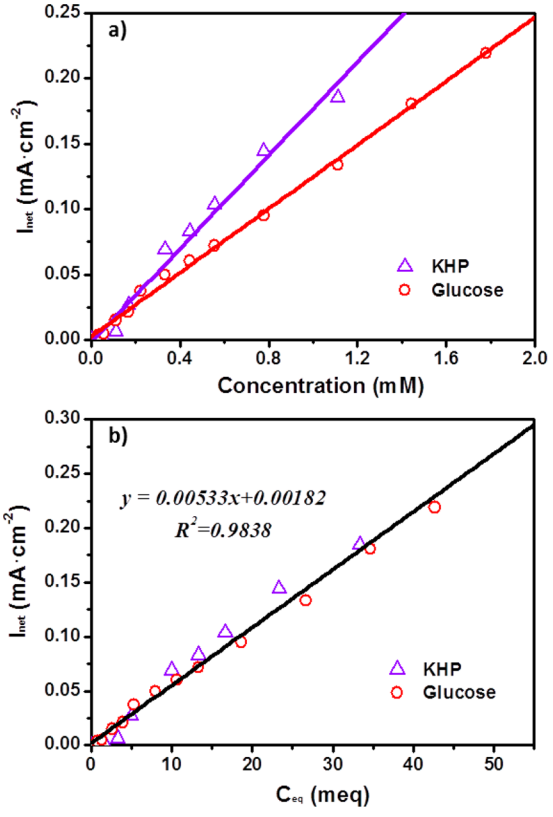

Figure 7. Relationships between I_{net} and the concentration of the H-TNTs electrodes, where C_{eq} (meq) = nC_M (mM).

number of KHP (30 e) than glucose (24 e). Using the data in Figure 7a, molar equivalent concentrations (C_{eq}, with a unit of meq) can be calculated by molar concentration (C_M) with its corresponding n, eq 9.

$$C_{eq} = nC_M \quad (9)$$

Subsequently, the I_{net} value of glucose and KHP were normalized and plotted against C_{eq} (Figure 7b). As expected,

the linear fit of the data (in 0−45 meq) resulted in an a R^2 value of 0.9838. The excellent linear relationship suggests that the H-TNTs photoanode is able to indiscriminately oxidize both types of organic compounds to the same extent (to water and CO_2) regardless of its identity and adsorptivity to the TiO_2 surface. This process is equivalent to "wet burning" of the organic compounds at the photoanode surface. The linear relationship is of primary importance to analytical chemistry because it enables the H-TNTs electrode to detect not only an individual organic compound but also aggregative parameters of organic compounds (e.g., COD in wastewater). This characteristic allows the H-TNTs to work as a universal sensor of organic compounds and provides a significant analytical principle for sensing applications using the PEC method with a high sensitivity and wide detection linear range.

4. CONCLUSIONS

The H-TNTs electrode has been successfully synthesized by the hydrogenation treatment of the TNTs. Because of the reduced band gap and the oxygen vacancies created via the hydrogenation process, the intrinsic electrochemical resistance of the TNTs is decreased and thus the PEC performance is significantly enhanced. A 2-fold higher PEC current value was obtained from the H-TNTs electrode compared with the TNTs electrode. The H-TNTs electrode therefore has the advantages of a higher sensitivity and wider linear range for the determination of organic compounds in aqueous solutions. Taking all of these factors into consideration, H-TNTs could be adopted as a promising electrode material for PEC sensors for organic compounds.

■ ASSOCIATED CONTENT

Ⓢ Supporting Information

Experimental setup for X-ray photoelectron spectrometer, XPS survey spectra of the TNTs and H-TNTs samples, and plot of I_{net} against glucose concentration for TNTs. This material is available free of charge via the Internet at http://pubs.acs.org.

■ AUTHOR INFORMATION

Corresponding Author

*E-mail: s.zhang@griffith.edu.au. Tel: 61-7-55528155. Fax: 61-7-55528067.

Notes

The authors declare no competing financial interest.

■ ACKNOWLEDGMENTS

We acknowledge the financial support from the Australia Research Council Discovery Project and the National Natural Science Foundation of China (no. 21328301) and technical assistance from the Australian Microscopy & Microanalysis Research Facility (AMMRF) at the Centre for Microscopy and Microanalysis (CMM), the University of Queensland.

■ REFERENCES

(1) Qiu, J.; Zhang, S.; Zhao, H. *Sens. Actuators, B* **2011**, *160*, 875−890.
(2) Fujishima, A.; Honda, K. *Nature* **1972**, *238*, 37−38.
(3) Roy, P.; Berger, S.; Schmuki, P. *Angew. Chem., Int. Ed.* **2011**, *50*, 2904−2939.
(4) Chen, X.; Mao, S. S. *Chem. Rev.* **2007**, *107*, 2891−2959.
(5) Zhang, S.; Qiu, J.; Han, J.; Zhang, H.; Liu, P.; Zhang, S.; Peng, F.; Zhao, H. *Electrochem. Commun.* **2011**, *13*, 1151−1154.
(6) Zhang, S.; Peng, F.; Wang, H.; Yu, H.; Zhang, S.; Yang, J.; Zhao, H. *Catal. Commun.* **2011**, *12*, 689−693.
(7) Danon, A.; Bhattacharyya, K.; Vijayan, B. K.; Lu, J.; Sauter, D. J.; Gray, K. A.; Stair, P. C.; Weitz, E. *ACS Catal.* **2012**, *2*, 45−49.
(8) Lu, Z.; Yip, C.-T.; Wang, L.; Huang, H.; Zhou, L. *ChemPlusChem* **2012**, *77*, 991−1000.
(9) Kang, Q.; Cao, J.; Zhang, Y.; Liu, L.; Xu, H.; Ye, J. *J. Mater. Chem. A* **2013**, *1*, 5766−5774.
(10) Zheng, Q.; Zhou, B.; Bai, J.; Li, L.; Jin, Z.; Zhang, J.; Li, J.; Liu, Y.; Cai, W.; Zhu, X. *Adv. Mater.* **2008**, *20*, 1044−1049.
(11) Akl, A. A.; Kamal, H.; Abdel-Hady, K. *Appl. Surf. Sci.* **2006**, *252*, 8651−8656.
(12) Fabrega, C.; Hernandez-Ramirez, F.; Prades, J. D.; Jimenez-Diaz, R.; Andreu, T.; Morante, J. R. *Nanotechnology* **2010**, *21*, 445703.
(13) Tang, H.; Prasad, K.; Sanjines, R.; Schmid, P. E.; Levy, F. *J. Appl. Phys.* **1994**, *75*, 2042−2047.
(14) Hahn, R.; Schmidt-Stein, F.; Salonen, J.; Thiemann, S.; Song, Y.; Kunze, J.; Lehto, V. P.; Schmuki, P. *Angew. Chem., Int. Ed.* **2009**, *48*, 7236−7239.
(15) Macak, J. M.; Gong, B. G.; Hueppe, M.; Schmuki, P. *Adv. Mater.* **2007**, *19*, 3027−3031.
(16) Wang, G.; Wang, H.; Ling, Y.; Tang, Y.; Yang, X.; Fitzmorris, R. C.; Wang, C.; Zhang, J. Z.; Li, Y. *Nano Lett.* **2011**, *11*, 3026−3033.
(17) Chen, X.; Liu, L.; Yu, P. Y.; Mao, S. S. *Science* **2011**, *331*, 746−750.
(18) Lu, X.; Wang, G.; Zhai, T.; Yu, M.; Gan, J.; Tong, Y.; Li, Y. *Nano Lett.* **2012**, *12*, 1690−1696.
(19) Zuo, F.; Wang, L.; Wu, T.; Zhang, Z.; Borchardt, D.; Feng, P. *J. Am. Chem. Soc.* **2010**, *132*, 11856−11857.
(20) Naldoni, A.; Allieta, M.; Santangelo, S.; Marelli, M.; Fabbri, F.; Cappelli, S.; Bianchi, C. L.; Psaro, R.; Dal Santo, V. *J. Am. Chem. Soc.* **2012**, *134*, 7600−7603.
(21) Khader, M. M.; Kheiri, F. M. N.; El-Anadouli, B. E.; Ateya, B. G. *J. Phys. Chem.* **1993**, *97*, 6074−6077.
(22) Cronemeyer, D. *Phys. Rev.* **1959**, *113*, 1222−1226.
(23) Fabregat-Santiago, F.; Barea, E. M.; Bisquert, J.; Mor, G. K.; Shankar, K.; Grimes, C. A. *J. Am. Chem. Soc.* **2008**, *130*, 11312−11316.
(24) Wang, Z.; Yang, C.; Lin, T.; Yin, H.; Chen, P.; Wan, D.; Xu, F.; Huang, F.; Lin, J.; Xie, X.; Jiang, M. *Adv. Funct. Mater.* [Online early access]. DOI: 10.1002/adfm.201300486. Published Online May 17, **2013**.
(25) Gordon, T. R.; Cargnello, M.; Paik, T.; Mangolini, F.; Weber, R. T.; Fornasiero, P.; Murray, C. B. *J. Am. Chem. Soc.* **2012**, *134*, 6751−6761.
(26) Zhang, S.; Zhao, H.; Jiang, D.; John, R. *Anal. Chim. Acta* **2004**, *514*, 89−97.
(27) Han, Y.; Zhang, S.; Zhao, H.; Wen, W.; Zhang, H.; Wang, H.; Peng, F. *Langmuir* **2010**, *26*, 6033−6040.
(28) Li, L.; Zhang, S.; Zhao, H. *J. Electrochem. Soc.* **2011**, *656*, 211−217.
(29) Zhang, S.; Li, L.; Zhao, H. *Environ. Sci. Technol.* **2009**, *43*, 7810−7815.
(30) Li, L.; Yang, M.; Zhang, S.; Liu, P.; Li, G.; Wen, W.; Zhang, H.; Zhao, H. *Nanotechnology* **2010**, *21*, 485503.
(31) Yu, H.; Zhang, S.; Zhao, H.; Zhang, H. *Phys. Chem. Chem. Phys.* **2010**, *12*, 6625−6631.
(32) Jiang, D.; Zhao, H.; Zhang, S.; John, R. *J. Phys. Chem. B* **2003**, *107*, 12774−12780.
(33) Momma, K.; Izumi, F. *J. Appl. Crystallogr.* **2011**, *44*, 1272−1276.
(34) Jiang, D.; Zhang, S.; Zhao, H. *Environ. Sci. Technol.* **2006**, *41*, 303−308.
(35) Michelswirth, M.; Räkers, M.; Schäfer, C.; Mattay, J.; Neumann, M.; Heinzmann, U. *J. Phys. Chem. B* **2010**, *114*, 3482−3487.
(36) Xin, M.; Li, K.; Wang, H. *Appl. Surf. Sci.* **2009**, *256*, 1436−1442.
(37) Kim, S.; Choi, W. *Environ. Sci. Technol.* **2002**, *36*, 2019−2025.
(38) Zhang, S.; Wen, W.; Jiang, D.; Zhao, H.; John, R.; Wilson, G. J.; Will, G. D. *J. Photochem. Photobiol., A* **2006**, *179*, 305−313.
(39) Calvo, M. E.; Candal, R. J.; Bilmes, S. A. *Environ. Sci. Technol.* **2001**, *35*, 4132−4138.